4654 *Biochemistry* **2010,** *49,* 4654–4661
DOI: 10.1021/bi9021582

BIOCHEMISTRY
including biophysical chemistry & molecular biology
Article

Single Molecular Observation of Self-Regulated Kinesin Motility[†]

Tomonobu M. Watanabe,[‡,§] Toshio Yanagida,[‡,∥,⊥] and Atsuko H. Iwane*[,∥,⊥]

[‡]*WPI, Immunology Frontier Research Center, Osaka University, Osaka, Japan,* [§]*PRESTO, Japan Science and Technology Agency (JST), Honcho Kawaguchi, Saitama, Japan,* [∥]*Nanobiology Laboratories, Graduate School of Frontier Biosciences, Osaka University, Osaka, Japan, and* [⊥]*Department of Physiology, Division of Physiological Science, Graduate School of Medicine, Osaka University, Osaka, Japan*

Received January 15, 2010; Revised Manuscript Received April 13, 2010

ABSTRACT: Kinesin-1 is an ATP-driven molecular motor that transports various cargoes in cells, a process that can be regulated by the kinesin tail domain. Here, kinesin ATPase activity and motility were inhibited *in vitro* by interacting the kinesin heavy chain C-terminal tail domain with the kinesin N-terminal motor domain. Though the tail domain can directly interact with microtubules, we found 70% of tail domains failed to bind in the presence of >100 mM (high) KCl, which also modulated the ATPase inhibition manner. These observations suggest that self-inhibition of kinesin depends on electrostatic interactions between the motor domain, the tail domain, and a microtubule. Furthermore, we observed self-regulated behavior of kinesin at the single molecule level. The tail domain did not affect motility velocity, but it did lower the binding affinity of the motor domain to the microtubule. The decrement in binding was coupled to ATPase inhibition. Meanwhile, the tail domain transfected into living cells not only failed to bind to microtubules but also inhibited the motor domain and microtubule interaction, in agreement with our *in vitro* results. Furthermore, at high potassium concentrations, the self-regulation of kinesin observed in cells was like that *in vitro*. The results favor a way tail inhibition mechanism where the tail domain masks the microtubule binding site of the motor domain in high potassium concentration.

Conventional kinesin (kinesin-1) is a motor protein that moves along microtubules by using the energy from ATP[1] hydrolysis in order to transport membrane-bound proteins and synaptic vesicles in cells (*1*, *2*). It works as a tetramer composed of two heavy chains (120 kDa each) and two light chains (60 kDa each) (*3*, *4*). Each heavy chain has a motor domain (amino acids 1−340) that is composed of at least one microtubule binding domain and a catalytic core which hydrolyzes ATP at the N-terminus (*5*), a global tail domain which binds cargoes (*6*, *7*) at the C-terminus, and a long α-helical coiled-coil region between the motor and the tail domains (*8*). There are several flexible sites, or hinges, which enable kinesin to form compactly within its long α-helical coiled-coil region. Although the light chains bind near the tail domains and play important functions *in vivo* (*9*−*11*), they are inconsequential to kinesin motility (*12*).

Of particular interest are the hinge sites. When kinesin is compactly folded at these sites, ATP hydrolysis and kinesin motility are greatly suppressed (*13*−*15*). When the tail domain without cargo approaches the motor domain (folded form), ATPase activity dramatically decreases due to the inhibition of ADP release (*16*). Cargo binding to the tail domain causes the tail domain to release from the motor domain (unfolded form), activating both ATPase and kinesin motility (*17*). Thus, kinesin motility is thought to be self-regulating by conforming between a folded and unfolded state.

More recently, the interaction of the tail domain and motor domain was structurally revealed using a cryoelectron microscope, indicating that the tail−motor interaction within kinesin is strikingly similar to the interaction of small GTPase and their regulators (*18*). This suggests that kinesin may share similar regulatory mechanisms with other p-loop proteins. Thus, the self-regulation of kinesin is a potential model for the operating principle behind NTPase proteins in general.

Currently, there are three widely accepted models explaining the self-regulation of kinesin motility. One has the tail domain mask the motor's microtubule binding sites such that it sterically blocks binding (Figure 1A, steric inhibition model) (*14*). Another argues that the tail domain represses an essential motor domain conformational change during motility (Figure 1B, allosteric inhibition model) (*16*). The last model assumes that one kinesin motor domain is swung by the β-sheet linker (also known as the neck linker and is located immediately behind the motor domain) during the ATPase cycle causing the other motor domain to bind to the forward tubulin binding site in a manner that resembles human walking (*19*). This model argues that movement of the motor domain is inhibited by the tail domain binding to the neck linker such that the tail domain acts as an anchor, inhibiting kinesin movement (Figure 1C, anchor model) (*20*). Regardless, the correct model should also incorporate the facts that the tail domain binds not only to the motor domain but also to the microtubule (*16*) and that full-length kinesin constructs can still move along microtubules, albeit less effectively (*20*).

To help identify which of these models is most appropriate, we prepared separate motor domains and tail domains to observe microtubule-stimulated kinesin ATPase and conducted single

[†]This work was supported by the Grant-in-Aid for Scientific Research and Technology program of the Japanese Science and Technology Corporation (PRESTO).

*Corresponding author. Tel: 81-6-6879-4632. Fax: 81-6-6879-4634. E-mail: a_iwane@fbs.osaka-u.ac.jp.

[1]Abbreviations: ATP, adenosine triphosphate; DK, *Drosophila* kinesin; EDTA, ethylenediaminetetraacetic acid; EGTA, ethylene glycol tetraacetic acid; GFP, green fluorescent protein; GST, glutatione *S*-transferase; SDS, sodium dodecyl sulfate; SIT, silicone target intensified tube.

 Published on Web 05/06/2010

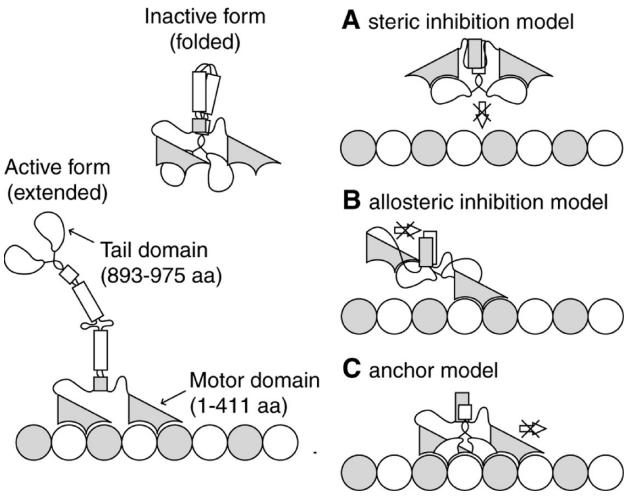

FIGURE 1: Schematic drawing of three different models for kinesin self-regulation by the tail domain. (A) Steric inhibition model. (B) Allosteric inhibition model. (C) Anchor model. See the introduction for details.

molecule imaging while altering the concentration of the tail domain and the assay conditions, especially the potassium chloride concentration. From these data, we propose a regulation model for kinesin motility dependent on the kinesin tail domain.

MATERIALS AND METHODS

Malachite Green and casein were obtained from Nakarai Tesque (Kyoto, Japan). PIPES, EDTA, and EGTA were obtained from Dojindo Laboratories (Kumamoto, Japan). Cy3 and Cy5 were obtained from Amersham Pharmacia Biotech UK (Poole, U.K.). All other chemicals were obtained from Sigma Chemical Co. (St. Louis, MO). All assays were performed at 25 °C. SDS−polyacrylamide gel electrophoresis (SDS−PAGE) was performed using a 15% separating gel.

Construction of Escherichia coli Expression Plasmids. Kinesin constructs were derived from the original *Drosophila* cDNA clone according to the method by Yang et al (*5*). The cDNA clone of DK411 (amino acids 3−411) was inserted into the *E. coli* expression vector pGEX-4T-1 (General Electric Healthcare Bio-Science Corp., NJ) at the *Xho*I site, as previously described (*21*). DK411 maintained its ability to move processively along microtubules and bind to the tail domain with binding site, which includes amino acids 357−367 (*17*). DK411 was constructed with glutathione *S*-transferase (GST) fusion protein at the N-terminus. To label at the C terminus with Cy3-maleimide, a reactivated cysteine-containing fragment, Leu-Gly-Pro-Gly-Gly-Gly-His-Arg-Lys-**Cys**-Phe, was introduced, as previously described (*22*). The cDNA clone of the DK893 tail encoded from amino acids 893−975 was inserted into the *E. coli* expression vector pET-28a (EMD Biosciences Inc., CA) at the *Nco*I−*Sca*I site. This construction encoded amino acids 927−945, which include the binding sites for both the motor domain and microtubules (*16*). The DK893 tail was constructed with a histidine tag at the N-terminus.

Protein Expression and Purification. DK411 were prepared and labeled with Cy3, as previously described (*22*). The Cy3/peptide ratio of DK411-bound Cy3, estimated from Cy3 and the peptide concentration of DK411, was determined by FluorImager595 (Molecular Dynamics, Sunnyvale, CA) and kept at < 0.3 to avoid motility inactivation (*22*). The DK893 tail was expressed in *E. coli*. BL21(DE3)pLysS and purified by histidine tag affinity chromatography. The BL21 harvest was lysed in 10 mL/g wet cells using lysis solution (50 mM PIPES−KOH, 150 mM NaCl, 20 mM imidazole, pH 7.5) and sonicated four times for 30 s on ice. The supernatant of this solution centrifuged at 20000*g* for 20 min at 4 °C was bound to 250 μL of His-Bind resin (Novagen, Germany) for 60−90 min also at 4 °C. The resin was loaded into a column and washed two times with 10 mL of wash solution 1 (50 mM PIPES−KOH, 150 mM NaCl, 50 mM imidazole, pH 7.5) and one time with 10 mL of wash solution 2 (50 mM PIPES−KOH, 150 mM NaCl, 80 mM imidazole, pH 7.5) to remove nonspecifically bound proteins. The DK893 tail was eluted with elution solution (50 mM PIPES−KOH, 150 mM NaCl, 100−300 mM imidazole, pH 6.8). A higher protein concentration (> 10 μM) fraction was dialyzed three times with dialysis solution (12 mM PIPES−KOH, 2 mM $MgCl_2$, 1 mM EGTA, pH 6.8) for 2 h at 4 °C. Part of the DK893 tail was labeled with Cy3 at the N-terminus. The Cy3/peptide ratio estimated from Cy3 and the peptide concentration of the DK893 tail was approximately 1.0.

ATPase Assays. The microtubule-stimulated ATPase of DK411 was measured by a modified Malachite Green method (*23*). The ATPase activity of 10 nM unlabeled DK411 was measured in 0−1 μM tail domains (DK893 tail), 0−5 μM microtubules, 0−150 mM KCl, 1 μM Taxol, and 1 mM ATP in 12 mM PIPES−KOH, 2 mM $MgCl_2$, and 1 mM EGTA, pH 6.8 at 25 °C, and determined by acquiring P_i release data at 30, 90, 150, 210, 270, and 330 s. Data were fitted with a least-squares method.

Cosedimentation Assays of the Kinesin Tail Domain and Microtubules. Kinesin tails bound to microtubules were separated from unbound tails by centrifugation. Samples of the DK893 tail and microtubules were mixed in 12 mM PIPES−KOH, 2 mM $MgCl_2$, and 1 mM EGTA, pH 6.8, at various potassium chloride concentrations, incubated at 25 °C for 15 min, and centrifuged at 400000*g* for 10 min at 25 °C. The extracts of the supernatant and pellet were analyzed by SDS−PAGE. The quantity of the tail domain bound to the microtubules was calculated from the intensity of the CBB staining using the public domain program Scion Image.

Single-Motor Motility Assays. Single-motor motility assays were performed according to previous methods (*22*). A flow chamber was made by placing a 25 μm × 18 mm × 9 mm glass plate over a cleaned quartz slide with two spacers in between. Cy5-labeled microtubules (20 μg/mL) were applied to the chamber. Microtubules were fixed onto the glass surface. After 5 min, nonbound microtubules in the chamber were washed out with casein solution (10 mM Trizma base, 100 mM NaCl, 5 mg/mL casein). The glass surface was coated with casein to avoid nonspecific binding of DK411. After unbound casein was removed by washing with assay solution (1 mM ATP, 50 mM KCl, 0.5% β-mercaptoethanol, and oxygen scavenger system in 20 mM PIPES−KOH, 10 mM potassium acetate, 4 mM $MgCl_2$, 2 mM EGTA, 0.2 mM EDTA, pH 6.8), kinesin solution (1 nM DK411, 0−1000 nM DK893 tail plus assay solution) was loaded onto the chamber (*24*). Observations were performed by using a total internal reflection fluorescence microscope at 25 °C (*25*).

Optics and Image Analysis. An $\sim 50 \times 50$ μm^2 area was illuminated by a green laser (532 nm; CrystaLaser, NV). Cy3 fluorescence was filtered using a high-pass wavelength filter (transmission wavelength = 580−630 nm; Asahi Spectra Co., Japan) and imaged by a GenIV image intensifier (VH4-1845; Videoscope, Ontario, Canada) coupled with a SIT camera

(Hamamatsu Photonics, Japan) at video rate. A low-pass filter was used on noisy image data to identify the location of Cy5-labeled microtubules. After contrast enhancement by an Argus-20 image processor (Hamamatsu Photonics), the image was recorded by a digital video recorder DSR-20 (Sony, Japan) for later analysis.

Image analysis was performed by using custom-made software. Fluorescence intensities were obtained using a rolling eight-frame average, which reduced the fluctuations by summing the intensities of an 8×8 pixel window and reduced the background intensity. DK411 positions were measured from the centroid of the fluorescent spots. Standard deviations of the position of DK411 rigidly attached to the glass surface were 25−35 nm. Nonspecific binding of DK411 to the glass surface was observed, but the binding duration was less than 100 ms. In order to distinguish precisely between nonspecific binding and microtubule binding, we defined the former as the disappearance of the fluorescence intensity within four frames (132 ms). A computer program was used to judge DK411 attachments and detachments to the microtubule to avoid experimenter bias. The travel distance was defined as the distance from the association to the dissociation of DK411 and microtubule. The velocity was estimated by tracking the motility and then applying a linear least-squares method to the trace.

Cotransfection of DK411 and the DK893 Tail into a Living Cell. pDK411−AcGFP: The DK411 cDNA clone (amino acids 3−411) was inserted into the mammalian N-terminal fusion protein with the GFP expression vector pAcGFP-N1 (BD Biosciences) at the *Bgl*II site. pmCherry−DK893 tail: The coding sequence for mCherry (*Bgl*II−*Age*I fragment) was obtained from the mammalian expression plasmid pmCherry-C1 (BD Biosciences). After the cDNA clone of DK (893 tail) was inserted into the mammalian C-terminal fusion protein with the GFP expression vector pAcGFP-C2 (BD Biosciences) at the *Eco*RI site, we exchanged the mCherry coding sequence for the AcGFP coding sequence in a manner that prevented any coding frame shift. A glycine-rich flexible chain DNA fragment was created by annealing the two oligonucleotides G-rich FC forward (5′ GATCTTGGGTGGTGGTGGTGACGACGCTCCTGGTG 3′) and G-rich FC reverse (5′ AATTCACCAGGAGCGTCGTCACCACCACCACCCAA 3′). The fragment was then inserted between the *Bgl*II and *Eco*RI sites between the mCherry and DK (893 tail) genes. Cotransfection assay: African green monkey kidney Cos-7 cells (American Type Culture Collection) were cultured in Dulbecco's modified Eagle's medium supplemented with 10% fetal calf serum. Transient transfections were done with Fugene-6 (Roche Biochemicals, Switzerland) according to the manufacturer's instructions. DNA concentration was 0.02 μg/μL. Twenty-seven hours after cotransfection, cells were trypsinized and replated on Matrigel (BD Biosciences) coated coverslips and incubated for 3−7 h.

RESULTS

Effect of Potassium Chloride on the Tail Domain Binding to Microtubules and on ATPase. We constructed DK411 and the DK893 tail from *Drosophila*'s kinesin heavy chain. The 357−367 amino acid region of DK411 is a binding site for the 937−945 amino acid fragment of the DK893 tail (*14*). The microtubule-stimulated ATPase of DK411 was inhibited by adding the DK893 tail (Supporting Information Figure S1 and Table 1), as seen in previous reports (*14*, *16*). V_{max} (saturation of ATPase activity) decreased as the exogenous DK893 tail concentration increased but was never fully inhibited. On the other hand, K_m (half-maximal ATPase rate) was unaffected by the DK893 tail.

Table 1: Tail-Mediated Inhibition of Microtubule-Stimulated ATPase

DK893 tail (nM)	KCl (mM)	V_{max}[a] (1/mol/head/s)	K_m[a] (μM)
0	0	23.4	0.71
0	50	24.6	1.3
0	150	22.2	1.6
300	0	14.0	0.37
300	50	11.8	1.4
300	150	10.5	1.4
500	50	9.8	1.3
1000	50	2.4	1.3

[a] V_{max} and K_m values were calculated by a least-squares method and averaged over four or five different measurements.

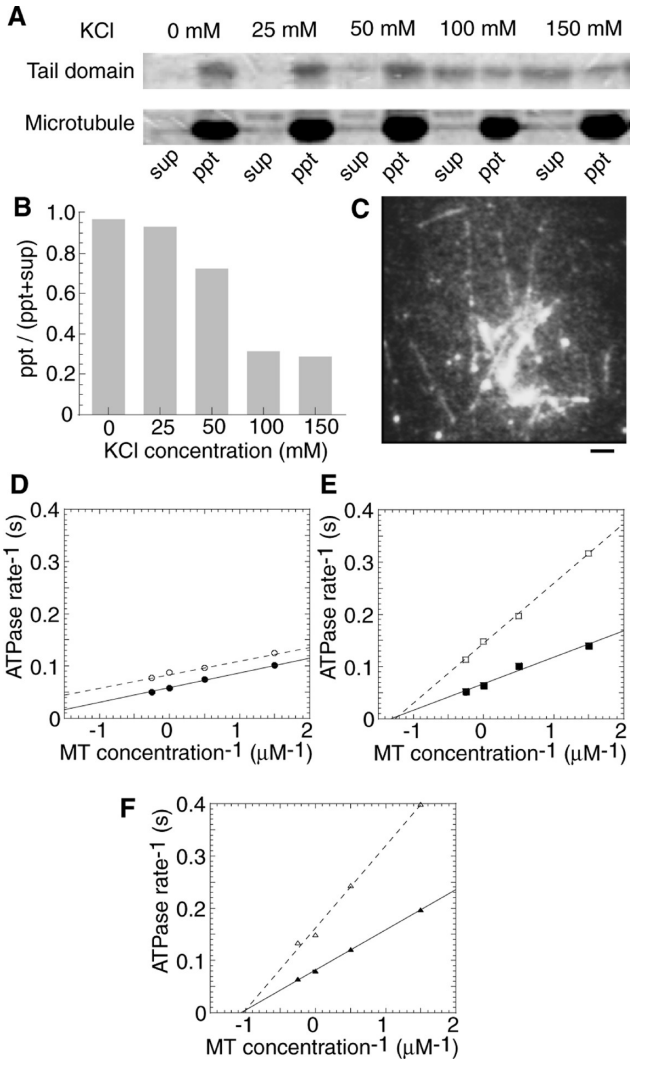

FIGURE 2: Potassium chloride concentration dependence of the DK893 tail binding to microtubules and its inhibition of ATPase. (A) Dependence at various potassium chloride concentrations from cosedimentation assays. The binding affinity decreased with an increase in potassium chloride concentration. (B) Ratio between ppt to ppt + sup in (A). (C) Fluorescent image of the Cy3-labeled tail domain while bound to microtubules at 0 mM KCl. Bar represents 2 μm. (D−F) Effect of potassium ion on inhibition (Lineweaver−Burk plot) at 0 (D), 50 (E), and 150 mM KCl (F). Solid lines indicate ATPase in the absence of the DK893 tail; broken lines indicate ATPase in the presence of 300 nM DK893 tail. See Table 1 for V_{max} and K_m.

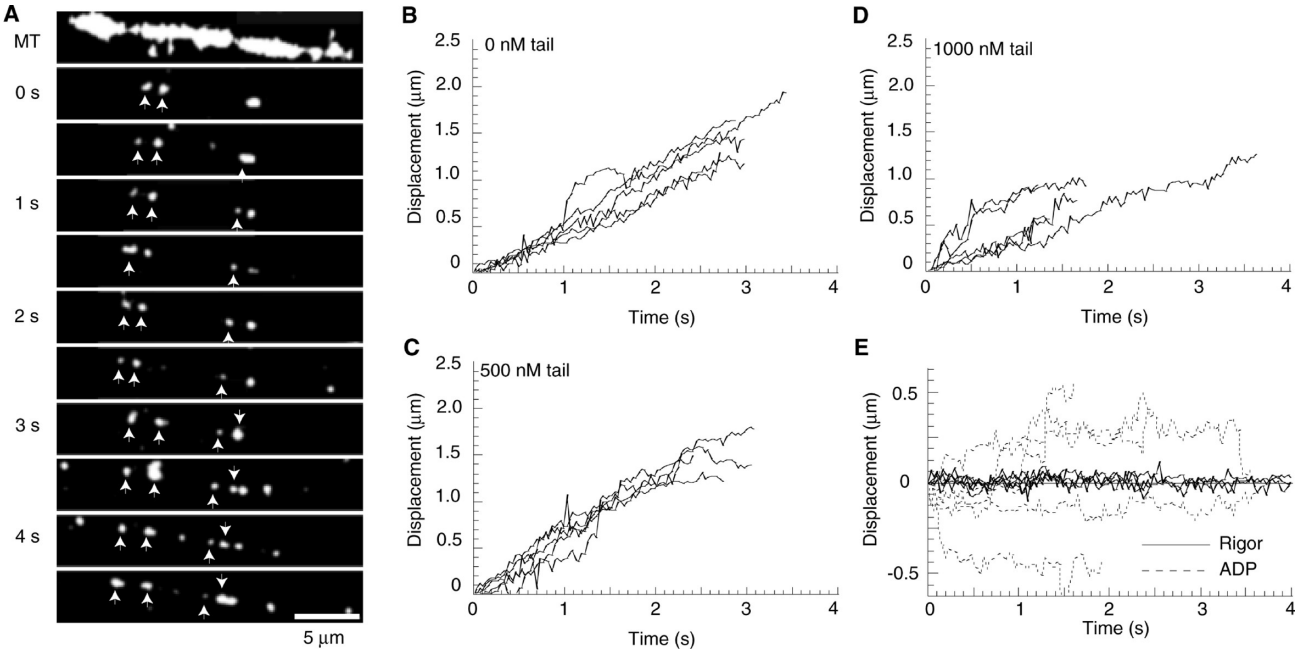

FIGURE 3: Movement of a self-regulated motor domain under a total internal fluorescence microscope. (A) Sequential images of a single Cy3-labeled DK411 moving along a microtubule. Processively moving DK411s are shown by arrows. (B−D) Five typical traces of the motor domain at 1 mM ATP in the absence (0 nM (B)) and presence of the DK893 tail (500 nM (C) and 1000 nM (D)). (E) Five typical traces of the motor domain in the rigor state (solid lines) and ADP state (broken lines) at 0 nM DK893 tail.

It has been reported that the tail fragment including the 897−911 amino acid fragment could bind to microtubules *in vitro* (*16*, *26*). But if this binding competed with DK411, then increasing DK411 should result in a subsequent increase in K_m of the microtubule-stimulated ATPase, which we did not observe, which indicates noncompetitive inhibition. We suspected that the inhibition manner depends on the solution condition, especially salt concentration. Therefore, we carried out cosedimentation assays of microtubules and the DK893 tail at various potassium chloride concentrations (0−150 mM KCl) (Figure 2A). Fewer than 10% of the DK893 tail failed to bind to microtubules at 0 or 25 mM KCl, approximately 30% failed at 50 mM KCl, and 70% failed at 100 and 150 mM KCl (Figure 2B). These results indicate that the DK893 tail binds to microtubules in a potassium chloride concentration-dependent manner. To confirm that these results were due to the DK893 tail domain binding to the microtubule and not some artifact, we directly observed the interaction under a fluorescent microscope (Figure 2C).

To investigate the effect of potassium chloride concentration on tail-mediated inhibition of microtubule-stimulated ATPase, we measured microtubule-stimulated ATPase at various potassium chloride concentrations in the presence of 300 nM DK893 tail (Figure 2D−F and Table 1). At 50 and 150 mM KCl, V_{max} was approximately half that in the absence of the DK893 tail going from 24.6 to 11.8 head/s/mol and 22.2 to 10.5 head/s/mol, respectively (Figure 2E,F), whereas K_m was unchanged (Table 1). In contrast, both V_{max} and K_m decreased at 0 mM KCl when changing the DK893 tail concentration from 0 to 300 nM from V_{max} = 23.4 to 14.0 head/s/mol and K_m = 0.71−0.37 μM, respectively (Figure 2D). Since Dietrich and colleagues have directly observed that the tail domain simultaneously contacts the kinesin-1 head and the microtubule at lower ionic strength (15 mM NaCl + 15 mM imidazole) by electron cryomicroscopy (*18*), it follows that the DK893 tail is involved in cross-linking DK411 to the microtubules, which in turn increases the DK411 affinity for microtubules during the ATPase assay. On the other hand, the tail domain had a much higher affinity for the motor domain than the microtubule at high potassium chloride concentration (> 50 mM KCl; data not shown), as previously reported (*14*). This did not, however, affect the motor's affinity for the microtubule.

Motility of Individual Self-Regulated Kinesin. Fluorescently labeled DK411 movement was observed by using a total internal reflection fluorescent microscope (Figure 3). Unfortunately, we could not detect DK411 movement in 150 mM KCl because such high potassium chloride concentration decreased the probability of DK411 interaction with the microtubules. When the concentration of DK411 increased, signals from single fluorophores were buried in the background noise due to the high number of DK411 molecules in solution. Therefore, we used 50 mM KCl since the inhibition manner between 50 and 150 mM KCl was similar (Figure 2E,F) and found that Cy3-labeled DK411 moved processively along a microtubule (Figure 3A), much like that previously reported using lower potassium chloride concentration buffer (*20*−*23*). We added the DK893 tail into the assay solution to investigate its effects on DK411 motor motility in 1 mM ATP (Figure 3B−D). Even at 1000 nM DK893 tail, almost all fluorescent spots, all indicating DK411, moved unidirectionally and processively (Figure 3D). As a control, DK411 in the rigor state and ADP state were observed (Figure 3E). Both showed different behavior from ATP conditions.

If the DK893 tail anchored to both DK411 and the microtubule (Figure 1C), we would expect to observe still motions during DK411 movement, consistent with a previous report (*20*). However, these were not observed (Figure 3B−D). We speculate that the single molecular behaviors were sensitive to the buffer condition, as they were for the ATPase assay in solution kinetics. Hence, we also carried out single molecule motility assays at low potassium concentration (10 mM potassium acetate) (Supporting Information Figure S2). DK411 sometimes paused during its processive movement along a microtubule (Supporting Information

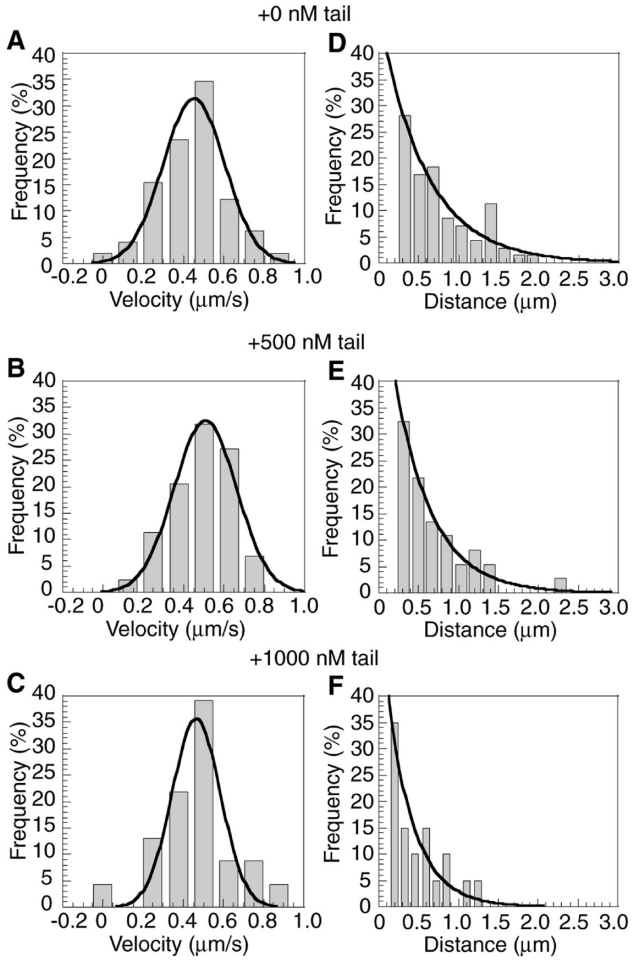

FIGURE 4: Effects of the DK893 tail on the velocity and travel distance of single DK411. The velocity (A−C) and travel distance (D−F) of an individual Cy3-labeled motor domain were determined from the traces in Figure 3B−D. The histograms in (A)−(C) were fitted to a single Gaussian function with peaks of 0.45, 0.50, and 0.46 μm/s for (A)−(C), respectively. The histograms in (D)−(F) were fitted to a single exponential function with travel distances of 0.57, 0.4, and 0.39 μm, respectively.

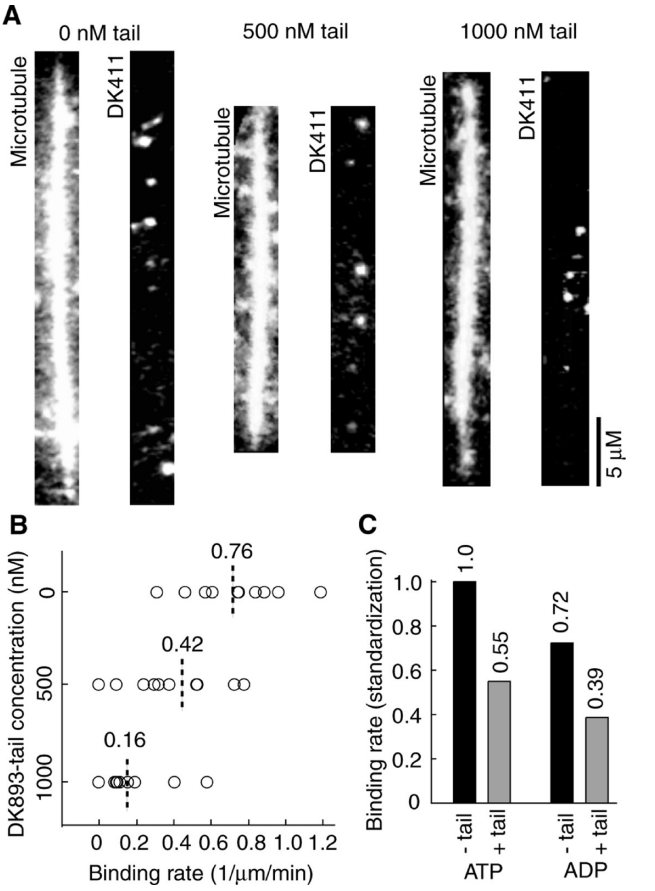

FIGURE 5: Inhibition of DK411 binding to microtubules. (A) Typical images of several DK411 bound to a microtubule. (B) Binding rate of DK411 to microtubules at various DK893 tail concentrations in 1 mM ATP. The binding rate of the moving DK411 to microtubules was defined as the number of DK411 molecules per 1 μm microtubule per 1 min. (C) Comparison of the binding rate in the presence of ATP and ADP. The binding rate was standardized.

Figure S2B, broken blue circles), again consistent with the previous report (*20*). Thus, we speculate that the DK893 tail bound both DK411 and microtubule and prevented the DK411 of forward movements and conclude that the anchor model is inappropriate for explaining kinesin's tail-mediated inhibition at 50 mM KCl.

To investigate the motile properties of DK411 when inhibited by the DK893 tail, we analyzed the velocity and travel distance of Cy3-labeled DK411 in the absence and presence of the DK893 tail (Figure 4). The travel distance was defined as the distance between the sites where DK411 attaches to and detaches from the microtubule. The velocity of DK411 distributed as a single Gaussian function with a peak at 0.52 μm/s (Figure 4A). The addition of the DK893 tail did not affect DK411 velocity (Figure 4B,C). The constant velocity indicated that the DK893 tail did not inhibit the ATPase cycle of DK411 bound to the microtubule. Histograms of the travel distance at various DK893 tail concentrations are shown in Figure 4D−F. The average travel distances at 0, 500, and 1000 nM DK893 tail were 0.57, 0.47, and 0.39 μm, respectively. This decrease was most likely due to the DK893 tail being bound to the microtubule (Figure 2A,B). Although the travel distance decreased with increasing levels of the DK893 tail, the extent of the effect was less than that on ATPase in solution (Supporting Information Figure S1 and Table 1).

In contrast to the change in travel velocity, the binding rate of DK411 to microtubules decreased remarkably with the addition of the DK893 tail (Figure 5A). The binding rate was calculated as the frequency of 1 nM DK411 binding to 1 μm microtubule for 1 min. The binding rates in the presence of 0, 500, and 1000 nM DK893 tail were 0.76, 0.42, and 0.16 /μm/min, respectively. This suggests that the DK411−DK893 tail complex failed to bind to the microtubule or could associate and dissociate from the microtubule within 120 ms since we detected a fluorescent spot moving for four video frames (1 frame = 30 ms) (see Materials and Methods).

There remained two ways in which we believe the kinesin tail inhibits motility: by suppressing interaction between DK411 and the microtubule or promoting detachment. Assuming that the DK893 tail masks the microtubule binding site from DK411, inhibition of DK411−microtubule binding by the DK893 tail should not depend on the nucleotide state. Therefore, we investigated the effect of adding the DK893 tail against the binding of DK411 to microtubules while in the ADP state (Figure 5C). The binding rate decreased 2-fold upon adding 500 nM DK893 tail. Combining this with our single molecule imaging assay data led us to conclude that the DK893 tail inhibits interaction between the DK411 and microtubule but does not slow the ATPase cycle.

A decreased binding rate was observed also at 10 mM potassium acetate going from 0.78 to 0.33 /μm/min (Supporting Information Figure S2A,B), despite the concentration of the exogenous tail being only 30 nM. In this condition, the association time, which is proportional to the travel distance, also decreased (Supporting Information Figure S2E,F, 1.91−0.81 s). In conjunction with the results seen in Figure 2A−C, we conclude that the tail domains covered the surface of the microtubules.

Inhibition of the DK893 Tail against DK411 Binding Microtubule in Living Cells. Because at 150 mM KCl the DK893 tail inhibited the interaction between the DK411 and microtubules *in vitro,* we investigated if a similar effect occurs *in vivo*. By applying immunofluorescence, one report found indirectly that the tail domain does interact with microtubules in cells (*27*). We aimed to directly observe this interaction by transfecting mCherry−DK893 tail and DK411−AcGFP into Cos-7 cells and viewing under a confocal fluorescent microscope (Figure 6). The DK411−AcGFP expressed cell shows many lines labeled with GFP, indicating DK411 localized along the microtubules (Figure 6A). In the cell cotransfected with mCherry−DK893 tail and DK411−AcGFP, neither bound to microtubules, although they did show colocalization everywhere in the cell except at the nucleus (Figure 6B). Even a cotransfected cell that expressed mCherry−DK893 tail at low levels showed microtubules labeled with DK411−AcGFP (Figure 6C). This was presumably the result of mCherry−DK893 tail binding to DK411−AcGFP, which prohibited the latter from binding to the microtubules.

DISCUSSION

In this study, we attempted to clarify the mechanism by which the kinesin tail domain inhibits the motility of its motor domain, finding that this inhibition depends on the potassium concentration (Figure 2). The number of tail domains bound to a microtubule dropped 70% in >100 mM KCl (Figure 2A,B) whereas its affinity for DK411 was relatively unaffected (*14*). Effects were also seen in ATPase (Figure 2D−F). At low K^+ concentration (< 50 mM), the tail domain could interact with both the motor domain and the microtubule (Figure 2) (*16*, *20*), which decreased the K_m of the microtubule-stimulated ATPase (Figure 2D). Furthermore, we observed "stop and go" movements by discrete DK411 at such concentrations (Supporting Information Figure S2). In combination, these results support the anchor model (Figure 1C). However, at high K^+ concentration (> 100 mM), the tail domain could anchor neither the motor domain nor a microtubule (Figure 4 and Supporting Information Figure S2), thus leaving K_m unchanged (Figure 2E,F). Furthermore, we did not see inhibited DK411 motility when using single molecule imaging. Along with the fact that we did not observe the obvious localization of the tail domain along microtubules in cells (Figure 6), our results suggest a large proportion of the kinesin tail domain does not bind to the microtubules but to the motor domain. Physiologically, we surmise that kinesin floats in the cytosol until it binds to a cargo but that weak binding by the tail domain to the microtubule keeps kinesin near the microtubule while awaiting its cargo.

In single molecule imaging observations, while the addition of the DK893 tail suppressed the binding of DK411 to the microtubules, it did not affect velocity (Figures 4 and 5). This suggests that the tail domain does not inhibit the motility of a microtubule-interacting motor domain and that the microtubule-stimulated

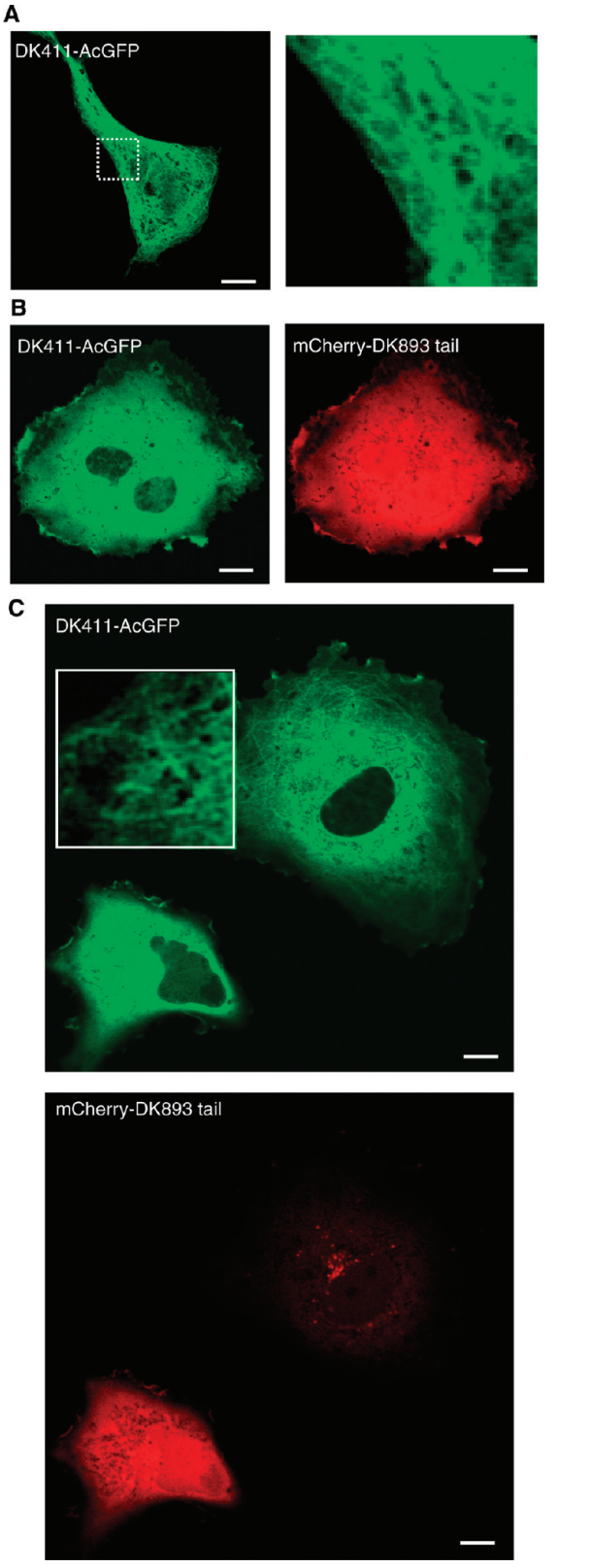

FIGURE 6: Localization of DK411−AcGFP and mCherry−DK893 tail in a Cos-7 cell. (A) Typical image of DK411−AcGFP localization in a Cos-7 cell. The right panel is a magnification of the area within the dotted white square in the left panel. (B) Typical image of DK411−AcGFP and mCherry−DK893 tail colocalization in a Cos-7 cell. (C) Typical image of DK411−AcGFP and mCherry−DK893 tail colocalization in a different Cos-7 cell. The inset panel is a magnification of part of the cell to the right where mCherry−DK893 tail was not seen to be sufficiently expressed. Bars represent 5 μm.

ATPase rate does not change. Furthermore, full-length, folded kinesin is known to detach from a microtubule in the presence of ATP but not in AMPPNP (*16*). Therefore, we argue that while the tail domain suppresses the interaction of the motor domain to the microtubule, it does not block the binding site completely. These observations can be described by the allosteric inhibition model (Figure 1B). Additionally, it was revealed that the tail domain inhibits Mg^{2+}-free ADP release in the absence of any microtubules (*28*) and that the tail domain directly interacts with the switch I region of the motor domain (*18*). Therefore, it is most likely that any conformational changes corresponding to ATP hydrolysis are suppressed by the tail domain.

We also estimated the apparent ATPase of a moving DK411 molecule in the single molecule imaging assay. DK411 moves processively with successive 8 nm steps, and each step couples with one ATP hydrolysis (*29*). Knowing this and noting that because the ATPase of the motor domain is activated only when the motor domain interacts with a microtubule, unlike the case for *in vitro* experiments, the apparent ATPase is calculated as (velocity)/(unitary step size) × (binding rate) × (travel distance), which decreased from 24.4/s in 0 nM DK893 tail to 3.6/s in 1000 nM DK893 tail. The ratio of these two values (0.15 = 3.6/24.4) is in good agreement with our solution assay (V_{max} ratio: 0.10 = 2.4/24.6, Table 1). Therefore, single molecule imaging observations reflected the ATPase inhibition observed in bulk assays.

Still, the allosteric inhibition model has its flaws. According to this model, the DK411−DK893 tail complex should adopt the behavior of DK411 with no tail in the ADP state since DK411 with the DK893 tail maintains the ability to bind to a microtubule and ADP. However, although we observed one-dimensional diffusions by DK411 for ~0.5 μm along a microtubule in 1 mM ADP (Figure 3E), we saw no such diffusions in 1 mM ATP and high DK893 tail concentrations (Figure 3D). Furthermore, a decrease in the binding rate by adding the DK893 tail was observed in 1 mM ADP (Figure 5C), which in combination with our imaging results implies the tail domain masks the microtubule binding site of the motor domain. Moreover, Hackney and colleagues reported that one tail domain in a dimer is sufficient to inhibit the ATPase activity of the two heads (*30*). This may cause the tail domain to inhibit only the back head while the front head is unaffected and can therefore bind to the microtubule, which will compromise processive movement (*20*, *21*, *31*).

In conclusion, combining previous reports with our present data leads us to believe a combination of the steric inhibition and allosteric inhibition models (Figure 1A,B) is best for describing the tail's regulation at physiological conditions while the anchor model applies at low potassium chloride conditions. This is in large part because the tail domain did not bind to microtubules in a cell (Figure 6) and that during motility the DK411−DK893 tail complex does not interact with the microtubule but instead dissociates into its subunits, allowing free DK411 to interact instead. Upon binding to a microtubule, DK411 cannot be bound by the DK893 tail due to steric limitations enabling DK411 to move processively. However, the DK893 tail can still weakly bind to a microtubule to disrupt DK411 motility. In the ATP state, this ability results in the lead head pushing the rear head forward (*32*, *33*) such that the tail domain inhibits only the rear head, which leads to premature dissociation and no processive movement.

In living cells, it is most likely that kinesin floats in the cytosol without interacting to a microtubule while awaiting cargo to bind. Once cargo does bind, however, we speculate that the tail domain dissociates from the motor domain, allowing kinesin to bind to and move processively along the microtubule in order to transport cargo to its intended destination. If true, this self-regulation would be an effective means to prevent kinesin from hydrolyzing ATP unnecessarily when no cargo is being carried. To confirm this regulation, future studies will need to examine whether the tail domain interacts with the motor domain within full-length kinesin inside a living cell.

ACKNOWLEDGMENT

We thank Dr. L. S. Goldstein for the gift of the *Drosophila* kinesin cDNA and P. Karagiannis for reading the manuscript.

SUPPORTING INFORMATION AVAILABLE

Figures S1 and S2 showing the DK893-tail concentration effect on microtubule-stimulated DK411 ATPase activity and single molecule imaging of Cy3-labeled DK411 at low ionic strength (50 mM potassium acetate), respectively. This material is available free of charge via the Internet at http://pubs.acs.org.

REFERENCES

1. Vale, R. D., Reese, T. S., and Sheetz, M. P. (1985) Identification of a novel force-generating protein, kinesin, involved in microtubule-based motility. *Cell 42*, 39–50.
2. Hirokawa, N. (1998) Kinesin and dynein superfamily proteins and the mechanism of organelle transport. *Science 279*, 519–526.
3. Bloom, G. S., Wagner, M. C., Pfister, K. K., and Brady, S. T. (1988) Native structure and physical properties of bovine brain kinesin and identification of the ATP-binding subunit polypeptide. *Biochemistry 27*, 3409–3416.
4. Kuznetsov, S. A., Vaisberg, E. A., Shanina, N. A., Magretova, N. N., Chernyak, V. Y., and Gelfand, V. I. (1988) The quaternary structure of bovine brain kinesin. *EMBO J. 7*, 353–356.
5. Yang, J. T., Saxton, W. M., and Goldstein, L. S. (1988) Isolation and characterization of the gene encoding the heavy chain of Drosophila kinesin. *Proc. Natl. Acad. Sci. U.S.A. 85*, 1864–1868.
6. Yang, J. T., Laymon, R. A., and Goldstein, L. S. (1989) A three-domain structure of kinesin heavy chain revealed by DNA sequence and microtubule binding analyses. *Cell 56*, 879–889.
7. Skoufias, D. A., Cole, D. G., Wedaman, K. P., and Scholey, J. M. (1994) The carboxyl-terminal domain of kinesin heavy chain is important for membrane binding. *J. Biol. Chem. 269*, 1477–1485.
8. de Cuevas, M., Tao, T., and Goldstein, L. S. (1992) Evidence that the stalk of *Drosophila* kinesin heavy chain is an alpha-helical coiled coil. *J. Cell Biol. 116*, 957–965.
9. Gindhart, J. G., Jr., Desai, C. J., Beushausen, S., Zinn, K., and Goldstein, L. S. (1998) Kinesin light chains are essential for axonal transport in *Drosophila*. *J. Cell Biol. 141*, 443–454.
10. Verhey, K. J., Lizotte, D. L., Abramson, T., Barenboim, L., Schnapp, B. J., and Rapoport, T. A. (1998) Light chain-dependent regulation of kinesin's interaction with microtubules. *J. Cell Biol. 143*, 1053–1066.
11. Rahman, A., Kamal, A., Roberts, E. A., and Goldstein, L. S. (1999) Defective kinesin heavy chain behavior in mouse kinesin light chain mutants. *J. Cell Biol. 146*, 1277–1288.
12. Yang, J. T., Saxton, W. M., Stewart, R. J., Raff, E. C., and Goldstein, L. S. (1990) Evidence that the head of kinesin is sufficient for force generation and motility in vitro. *Science 249*, 42–47.
13. Hackney, D. D., Levitt, J. D., and Suhan, J. (1992) Kinesin undergoes a 9 to 6 S conformational transition. *J. Biol. Chem. 267*, 8696–8701.
14. Stock, M. F., Guerrero, J., Cobb, B., Eggers, C. T., Huang, T. G., Li, X., and Hackney, D. D. (1999) Formation of the compact confomer of kinesin requires a COOH-terminal heavy chain domain and inhibits microtubule-stimulated ATPase activity. *J. Biol. Chem. 274*, 14617–14623.
15. Cross, R., and Scholey, J. (1999) Kinesin: the tail unfolds. *Nat. Cell Biol. 1*, E119–121.
16. Hackney, D. D., and Stock, M. F. (2000) Kinesin's IAK tail domain inhibits initial microtubule-stimulated ADP release. *Nat. Cell Biol. 2*, 257–260.

17. Coy, D. L., Hancock, W. O., Wagenbach, M., and Howard, J. (1999) Kinesin's tail domain is an inhibitory regulator of the motor domain. *Nat. Cell Biol. 1*, 288–292.
18. Dietrich, K. A., Sindelar, C. V., Brewer, P. D., Downing, K. H., Cremo, C. R., and Rice, S. E. (2008) The kinesin-1 motor protein is regulated by a direct interaction of its head and tail. *Proc. Natl. Acad. Sci. U.S.A. 105*, 8938–8943.
19. Sellers, J. R. (1996) Kinesin and NCD, two structural cousins of myosin. *J. Muscle Res. Cell Motil. 17*, 173–175.
20. Friedman, D. S., and Vale, R. D. (1999) Single-molecule analysis of kinesin motility reveals regulation by the cargo-binding tail domain. *Nat. Cell Biol. 1*, 293–297.
21. Inoue, Y., Toyoshima, Y. Y., Iwane, A. H., Morimoto, S., Higuchi, H., and Yanagida, T. (1997) Movements of truncated kinesin fragments with a short or an artificial flexible neck. *Proc. Natl. Acad. Sci. U.S.A. 94*, 7275–7280.
22. Inoue, Y., Iwane, A. H., Miyai, T., Muto, E., and Yanagida, T. (2001) Motility of single one-headed kinesin molecules along microtubules. *Biophys. J. 81*, 2838–2850.
23. Iwatani, S., Iwane, A. H., Higuchi, H., Ishii, Y., and Yanagida, T. (1999) Mechanical and chemical properties of cysteine-modified kinesin molecules. *Biochemistry 38*, 10318–10323.
24. Harada, Y., Sakurada, K., Aoki, T., Thomas, D. D., and Yanagida, T. (1990) Mechanochemical coupling in actomyosin energy transduction studied by in vitro movement assay. *J. Mol. Biol. 216*, 49–68.
25. Funatsu, T., Harada, Y., Tokunaga, M., Saito, K., and Yanagida, T. (1995) Imaging of single fluorescent molecules and individual ATP turnovers by single myosin molecules in aqueous solution. *Nature 374*, 555–559.
26. Yonekura, H., Nomura, A., Ozawa, H., Tatsu, Y., Yumoto, N., and Uyeda, T. Q. (2006) Mechanism of tail-mediated inhibition of kinesin activities studied using synthetic peptides. *Biochem. Biophys. Res. Commun. 343*, 420–427.
27. Navone, F., Niclas, J., Hom-Booher, N., Sparks, L., Bernstein, H. D., McCaffrey, G., and Vale, R. D. (1992) Cloning and expression of a human kinesin heavy chain gene: interaction of the COOH-terminal domain with cytoplasmic microtubules in transfected CV-1 cells. *J. Cell Biol. 117*, 1263–1275.
28. Hackney, D. D., and Stock, M. F. (2008) Kinesin tail domains and Mg^{2+} directly inhibit release of ADP from head domains in the absence of microtubules. *Biochemistry 47*, 7770–7778.
29. Schnitzer, M. J., and Block, S. M. (1997) Kinesin hydrolyses one ATP per 8-nm step. *Nature 388*, 386–390.
30. Hackney, D. D., Baek, N., and Snyder, A. C. (2009) Half-site inhibition of dimeric kinesin head domains by monomeric tail domains. *Biochemistry 48*, 3448–3456.
31. Kamei, T., Kakuta, S., and Higuchi, H. (2005) Biased binding of single molecules and continuous movement of multiple molecules of truncated single-headed kinesin. *Biophys. J. 88*, 2068–2077.
32. Vale, R. D., and Milligan, R. A. (2000) The way things move: looking under the hood of molecular motor proteins. *Science 288*, 88–95.
33. Mori, T., Vale, R. D., and Tomishige, M. (2007) How kinesin waits between steps. *Nature 450*, 750–754.